Identifying two ignition modes of polymer insulated wires with continuous excess current in microgravity

Feng Guo[a*], Seiya Kawaguchi[a], Nozomu Hashimoto[a], Osamu Fujita[a*]

[a]Division of Mechanical and Aerospace Engineering, Hokkaido University, Kita 13, Nishi 8, Kita-ku, Sapporo, Hokkaido, 060-8628, Japan

*Corresponding author.

Email address: cumt-guofeng@hotmail.com (F. Guo); ofujita@eng.hokudai.ac.jp (O. Fujita)

Highlights:

- 2-D simulations reproduced ignition delay with wide-range currents in microgravity.
- "Spontaneous ignition" and "wire assisted ignition" modes were identified.
- The transition and control mechanism of two ignition modes were discussed.
- Minimum ignition energy can be obtained in the mode of spontaneous ignition.

Abstract:

Overload ignition of electric wires in microgravity has been investigated for space fire safety. Microgravity experiments from drop towers and parabolic flight have been conducted to observe the overall ignition phenomena. Two-dimensional numerical simulations were performed employing finite-rate chemistries in both condensed and gas phases. As the applied current changes, two distinct ignition modes were found in both experiments and simulations, one away from the wire and the other near the wire surface, named "spontaneous ignition" and "wire assisted ignition", respectively. After validating ignition delay times by experiments, the simulation results were used to discuss the transition of two ignition modes. With a lower current, the spontaneous exothermic reaction at the pyrolysis gas front led to the far-distance ignition. While with a higher current, the local heat loss suppressed spontaneous ignition; meanwhile, the excessive heat from the exposed core wire caused the surface ignition. In addition, the ignition energy showed a non-monotonical increase with the applied current, where the minimum ignition energy was consumed with 5.5 A current supply implying the high fire risk of the "spontaneous ignition" regime. The control mechanisms of the ignition energy change in different stages were discussed.

Keywords: Wire fire; Modeling; Ignition; Microgravity; Overloading; Fire safety in space

1. Introduction

In addition to the current manned missions on the International Space Station (ISS), further manned space activities such as NASA's Artemis Program are expected to become more active in the future. Ensuring the fire safety of the crews is one of the most important issues to lead such projects to success. Many studies on the ignition of solid materials have been conducted in microgravity (μG) to prevent a fire in spacecraft, such as piloted ignition of Poly Methyl Methacrylate (PMMA) plates [1,2] and ignition of thin cellulosic [3–6] and PMMA sheets [7] by external radiation. As spacecrafts have massive electrical devices, the ignition of wire harnesses is the potential cause of electrical fires [8,9]. To observe the ignition behaviors of electric wires in μG, several experimental works have been conducted for laser piloted ignition [10,11] and smoke generation [12,13]. While our research group has carried out a series of studies focusing on the overload ignition of polymer-insulated wire in μG [14–17]. All the results showed that the ignition risk of electric wires dramatically increases in microgravity in comparison with normal gravity.

In our previous experimental findings [14,15], the limiting electric current to cause ignition can extend in μG with a lower current value and a longer delay time than that in normal gravity. We expected that if the μG time was long enough, an ultimate ignition limit could be found. At present, due to the high cost of long-term space experiments (on ISS or satellite) and the limitation of short-term ground experiments (by drop tower or parabolic flight), our understanding of the ignition mechanism of electric wire in reduced gravity is still limited. Therefore, numerical approaches are needed to clarify the ignition mechanism and predict the ultimate ignition limit of overloaded wires. In our past studies, a one-dimensional (1-D) numerical model had been developed to investigate overloaded wire ignition [16,17]. By carefully setting boundary conditions and employing single-step chemistry in solid and gas phases, the 1-D model qualitatively predicted the tendency of ignition delay and oxygen limits in μG [16]. The radiative heat loss from the wire insulation surface has been emphasized as a dominant heat loss when determining the ultimate ignition limit in long-term μG exposure [17].

Recently, an upgraded two-dimensional (2-D) numerical model was proposed utilizing the Fire Dynamics Simulator (FDS) [18], to improve the numerical prediction accuracy and for future application in different environment conditions (gravities, flow, or multiple wires). Prior to the partial gravity analysis, a μG condition facilitates the validation in a wide range of applied currents. In the recent 2-D numerical work focusing on pyrolysis parameters in μG [19], ignition occurred differently with the pyrolysis processes. It inspired us to clarify more insights into the ignition modes with different overload currents associated with the μG experiments. As the previous 1-D numerical study was limited to the low current cases near the ignition limit, the overload ignition phenomena with a wide range of electric currents have not been well clarified. In this paper, the effects of wide-range overload currents on the ignition characteristics of electric wires will be investigated through 2-D numerical simulations and μG experiments.

2. Experimental setup

The setup for the μG experiments is shown in Fig. 1. The wire sample with an effective length of 70mm is fixed in the center of the closed chamber by a wire holder and connected with the direct current power supply. The inside dimension of the chamber is 230 (W) × 140 (D) × 170 (H) mm. Direct imaging and backlight imaging can be recorded by the high-speed camera (1000 fps) through the window. To ensure successful ignition during a short-term μG environment, we used the laboratory wire sample with low-density polyethylene (LDPE) insulation which has a high flammability, and nichrome (NiCr) core wire, which has a high electrical resistance (R_0 = 5.5 Ω/m ± 7% at room temperature, corresponding to an electrical resistivity of 1.1×10^{-6} Ω·m). The insulation thickness (δ_{p0}) is 0.15 mm and the core radius (r_c) is 0.25 mm. Experimental data have been collected from three μ*G* experimental facilities, the specifications are shown in Table 1. Detailed experimental procedures can be found in the previous paper [15].

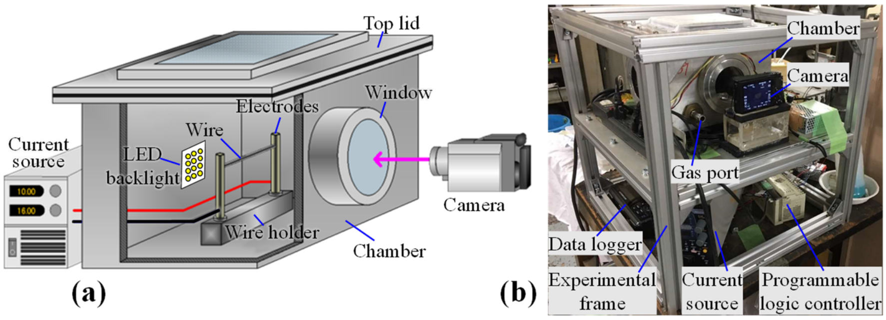

Fig.1. Experimental setup (a) schematic of experimental chamber, (b) overview picture.

Table 1. Specifications of microgravity facilities [14–17]

Facility name	Type	Location	*G*-quality	Duration
COSMOTORRE	45m drop tower	Hokkaido, Japan	$10^{-3}G$	2.5~3.0 s
MGLAB	100m drop tower	Gifu, Japan	$10^{-5}G$	4.5 s
DAS	Parabolic flight	Aichi, Japan	$3\times10^{-2}G$	~20 s

3 Numerical model

The numerical simulations are carried out utilizing FDS v6.7.1. The size of the computational domain is equivalent to the cross-section of the experimental chamber, which is under a 2-D Cartesian coordinates system with a uniform grid (square meshes), as shown in Fig. 2. The thickness of the 2-D domain (d_y) is 1 mm. The quiescent gas is sealed by an inert wall with constant temperature (T_w). The gravitational acceleration (g), initial oxygen fraction ($O_2\%$), initial ambient temperature (T_0), and pressure (P_0) were indicated in Fig.2 as well. The sensitivity analysis of the mesh resolution and corresponding computation time can be found in the Supplementary Material (S.1). For the balance of accuracy and computational cost, the adopted cell size was 0.4 mm, which has been confirmed well for related numerical studies for solid ignition [5]. The initial time step is 0.001s, it was automatically adjusted by restraining the Courant number lower than 0.8. Unless otherwise noted, the simulations used FDS default settings. Because the current was varied over a wide range, the typical computing time is in the range of 7 to 300 hours using an Intel Xeon W2255 CPU.

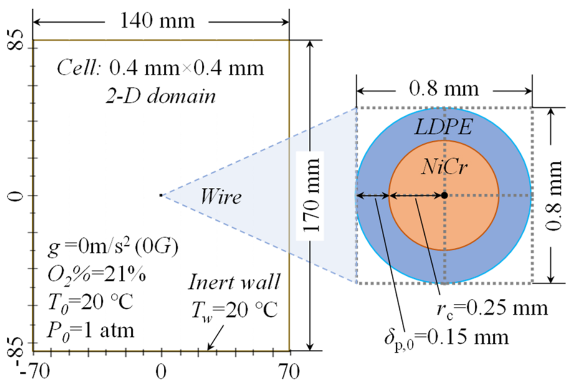

Fig. 2. Schematics of the 2-D computational domain.

The wire sample is located at the center of the domain. The surface boundaries of the wire have two layers with different material properties. The outer layer is solid LDPE (δ_{p0} = 0.15 mm), and the inner layer is NiCr core (r_c = 0.25 mm). It was noted that the 2-D simulation was performed under Large eddy simulation (LES) mode to allow the treatment of wire surface under cylindrical coordinates [18,20]. Although the geometric appearance of the wire boundaries matches with the square grid, boundary conditions including the empirical convection model on the wire surface and mass flux due to pyrolysis conform to the cylindrical coordinates, as well as the heat conduction equations in the solid. The default radiation model of FDS for the radiation transfer (optically thick, employing Specified Radiative Fraction) was adopted in this work. A volumetric internal heat source was applied to the inner layer to simulate Joule heat based on the overload current (I), which can be expressed as:

$$\dot{q}_{in}''' = \frac{R_0 I^2}{\pi r_c^2 d_y} \quad (1)$$

where R_0 is 5.5 Ω/m based on the wire sample specification [15]. Since to the measured electrical resistance of NiCr wire with different applied current has a small difference from the nominal value R_0 (as shown in the Supplementary Material S.2.), we assumed that the resistance is constant during overloading for simplicity. Such an internal heat source causes the melting of the solid LDPE first, then molten LDPE was pyrolyzed to the C_2H_4 monomers. In the phase change reaction (PCR) function of FDS 6.7.1, the melting process consumes the latent heat (H_m) of 140.6 kJ/kg at the melting temperature (T_m) of 118 °C referring to [21]. The physical properties were carefully examined and decided as following Table 2, identical to the previous work [19].

Table 2. Physical properties of materials used in simulations.

Properties \ materials	**NiCr**	**Solid LDPE**	**Molten LDPE**
Density (ρ) [kg/m^3]	8410	920	760 [22]
Specific heat (c) [kJ/(kg·K)]	0.481	2.3	2.5 [23]
Thermal conductivity (k) [W/(m·K)]	17.4	0.34	0.25 [24]
Emissivity (ε)	0.7	0.3 [25]	0.1 [26]

The pyrolysis is expressed as a single-step reaction to produce pure ethylene (without charring):

$$[\mathrm{LDPE}]_{\mathrm{molten}} \rightarrow [C_2H_4]_{\mathrm{gas}} \quad (2)$$

The pyrolysis reaction rate (r_s) follows the Arrhenius-type equation:

$$r_s = A\left(\frac{\rho_s}{\rho_{s0}}\right) \exp\left(-\frac{E}{RT_s}\right) \quad (3)$$

where pre-exponential factor $A = 5.0 \times 10^{18}$ s^{-1} and activation energy E = 300 kJ/mol are used based on thermalgravimetric analysis [19]. ρ_s is the insulation's density (kg/m^3), R is the gas constant (8.314 J/K/mol), and T_s is the insulation's temperature (K). The pyrolysis consumes the latent heat (H_r) of 962 kJ/kg [27]. After completing pyrolysis, the temperature of the core wire is used as the wire surface temperature. Note that in FDS 6.7.8 and later versions, Eq. (3) has been slightly modified by multiplying ρ_{s0} by the density term.

For the gas phase, the thermal properties and diffusion coefficients of the gas are computed by the molecular weights and Lennard-Jones parameters for nitrogen as an empirical function of temperature [20]. The combustion reaction is assumed to follow a single-step finite rate reaction:

$$C_2H_4 + 3O_2 \rightarrow 2CO_2 + 2H_2O \qquad (4)$$

The reaction rate is expressed as follows with the reaction order of 1.75 according to the work by Westbrook and Dryer [28]:

$$\frac{d[C_2H_4]}{dt} = -A_g \exp\left(-\frac{E_g}{RT_g}\right)[C_2H_4]^{0.1}\,[O_2]^{1.65} \qquad (5)$$

where gas-phase pre-exponential factor $A_g = 2.0\times10^{12}$ (mol/cm^3)$^{-0.75}$/s; gas-phase activation energy E_g = 125,520 J/mol (30 kcal/mol); T_g is the gas-phase temperature (K), $[C_2H_4]$ and $[O_2]$ are mole concentrations (mol/cm^3) of fuel and oxygen with different reaction orders, respectively. Since the temperature in a large-scale calculation can be smeared out over a mesh cell, the application of finite rate chemistry in LES should be careful. However, we assume that such effects are limited in the very small scale and mesh size model used here.

In this study, it is considered that ignition happens when the local volumetric heat release rate by the chemical reaction exceeds 32 MW/m^3 which is estimated from volumetric heat release by the stoichiometric reaction of ethylene and air at the auto-ignition temperature (815 K) [29]. The choice of the ignition criteria has been discussed in the previous work [19], which is in the reasonable order of magnitude according to related numerical works for solid ignition by Kashiwagi and Nakamura [5,30–32].

4 Results and discussions

4.1 Observation of two ignition modes

Ignition phenomena from experiments and simulations were compared to validate the new model. Figure 3 shows the experimental images around the ignition moments under the applied current of 5 A and 18 A, respectively. To clearly observe the ignition point, we used monochrome backlight images and color direct images for the case of 5 A and 18 A, respectively, where the red circles represent the ignition initiation point. In Fig. 3 (a), the core wire under 5 A current was partially exposed at 7.720 s due to molten balls of LDPE under surface tension, then ignition occurred spontaneously away from the wire at 7.736 s. In contrast, for the 18 A case in Fig. 3 (b), the exposed core wire glowed red and then ignited adjacent gases of the wire surface at 0.876 s, which implies that the high-temperature core wire assists the ignition. In both cases, flames propagated axially along the wire after ignition to form a tubular flame, which is unique to microgravity environments.

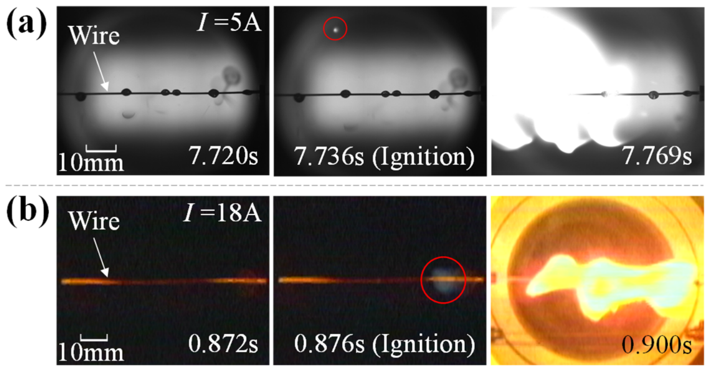

Fig. 3. Experimental images of wire ignition with applied current of (a) 5 A recorded by backlight image; (b) 18 A recorded by direct image.

Figure 4 shows the simulation images characterized by the heat release rate per unit volume (HRRPUV) at 5 A and 18 A applied current, respectively. The color bar indicates the magnitude of the HRRPUV caused by the gas phase reaction from 0 to 3.2 MW/m3 (the ignition criteria). Thus, the brightest part can represent the flame sheet. For the simulation results, ignition occurred about 7 mm away from the wire at 8.179 s under the 5 A applied current, while ignition occurred near the wire at 0.806 s under the 18 A applied current. In comparison, the magnitude of the ignition time and the tendency of the ignition positions of the simulations have good agreement with the experimental results. It was shown that the 2D simulation model can qualitatively reproduce the wire ignition phenomena in microgravity.

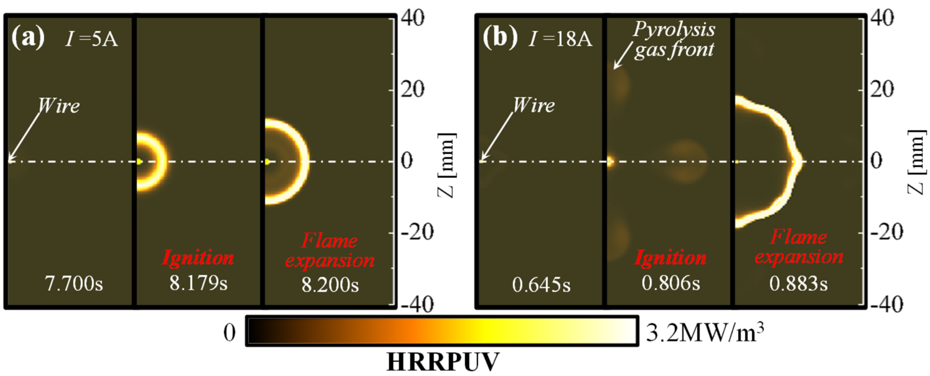

Fig. 4. Simulation images of wire ignition represented by HRRPUV with applied current of (a) 5 A and (b) 18 A.

Noted that when the applied current is very high, the angular dependence of the HRR evolution can be found in the 0G condition, which is believed to be caused by the square grid system in FDS. As discussed in the Supplementary Material (S.3), we assumed that the effect on the accuracy/applicability of this model is also limited in horizontal and vertical directions, thus the following radial data were acquired from the averaged value in vertical directions, which corresponds to the ignition delay and position.

4.2 Ignition delay times

For further validation, the ignition delay times (t_{ig}) of the experimental and simulation results were compared over a wide range of applied currents, defined as the elapsed time from the start of the electric current supply to the moment of ignition. As shown in Fig. 5, the colored open symbols represent the experimental results collected at different microgravity facilities [14,17], and the black circle symbols with the dashed line represent the 2D simulation results. Overall, the simulated ignition delay times show good agreement with the experimental data. The discrepancy becomes larger for low current cases near the ignition limit, possibly due to differences between the 2-D model and 3-D experiments, including the motion of the molten LDPE insulation along the wire and the complex flow field in the experiments. As can be seen in Fig. 3 (a), the partially exposed core wire can provide more heat to the gas phase due to the separation of the molten spheres under a lower current supply; but in the 2-D simulation, the core wire cannot be exposed until all the LDPE is pyrolyzed. The predicted limiting ignition current from the 2D simulation is about 2.9 A with a longer delay time (~33 s). However, the measurable ignition limit in experiments was about 3.5 A due to the time limitation (~20 s) of microgravity facilities. The final limit will be measured by space experiments planned on the ISS for further validation. Since the 2-D model reproduced the ignition phenomena and quantitatively predicted the ignition delay time under the validation of the experimental results, we will discuss the ignition characteristics mainly based on the simulation results.

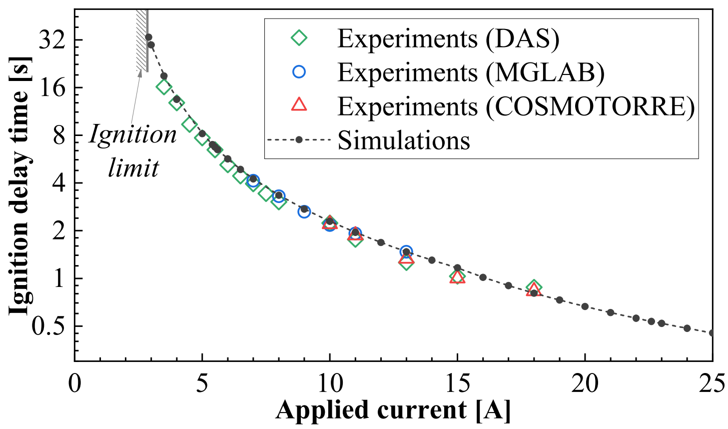

Fig. 5. Comparison of ignition delay times between μ*G* experiments and 2-D simulations as a function of applied current.

4.3 Transition of two ignition modes

Since we found different ignition initiation points in Fig. 3 and Fig. 4, the variation of ignition positions with different applied currents is of interest. Figure 6 (a) shows the radial ignition positions from the wire surface as a function of the applied current by simulation. The ignition initiation point was regarded as the nearest cell where HRRPUV exceeds the ignition criteria (3.2 MW/m^3). From Fig. 6 (a), the distance of the ignition position increases with the applied current, but the trend changes suddenly after the current exceeds 15A. We can distinguish the two ignition modes from the different manners of ignition positions. In the first regime, ignition occurs spontaneously away from the wire under a lower current supply, and the increased current expands the ignition position. In the second regime, ignition occurs close to the wire surface with a higher applied current. We will refer to these two ignition modes as the “spontaneous ignition” and “wire-assisted ignition” regimes.

To clarify the mechanism that makes two ignition modes, the time scales of the ignition delay (t_{ig}) and pyrolysis completion (t_p) were recorded. The ratio of t_{ig} and t_p as a function of applied current was plotted in Fig. 6 (b). When this ratio is higher than unity ($t_{ig}/t_p > 1$), the ignition happens after all the LDPE insulation pyrolyzes to the gas phase leading to the core wire exposure; otherwise ($t_{ig}/t_p < 1$), the ignition starts while the insulation is remaining. The “spontaneous ignition” regime can be divided into two parts by the boundary of $t_{ig}/t_p = 1$, ignition happens earlier (S-1) and later (S-2) than the pyrolysis completion. By contrast, the t_{ig}/t_p is always larger than unity in the “wire-assisted ignition” regime, that is, the core wire is already exposed before ignition. Combined with the ignition position in Fig. 6 (a), the released pyrolysis gas may ignite spontaneously in S-1, but the core wire exposure may have a negligible effect on the ignition far away from the wire in S-2. In the “wire-assisted ignition” regime, the exposure of high-temperature core wire may lead to a piloted ignition (hot-surface ignition). We will find more details to verify the above hypothesis in the following parts.

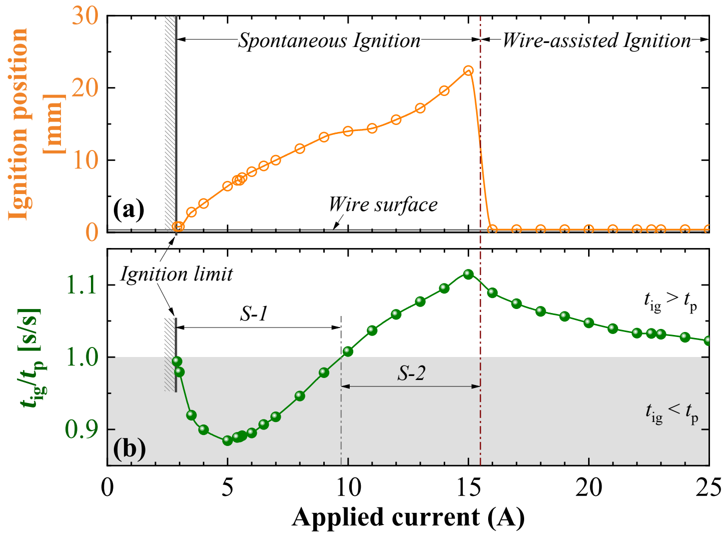

Fig. 6. Transition of two ignition modes as a function of applied current: (a) ignition position; (b) ratio of ignition delay time and pyrolysis completion time.

In S-1 of Fig. 6 (b) with a lower current supply, ignition occurred during the pyrolysis process. For the typical case with 5 A current, the distributions of HRRPUV, temperature, and reactant fractions along the radial direction around the ignition moment are plotted in Fig. 7 (a). According to the HRRPUV profile at 8.18 s, the ignition occurred at a distance of 6.2 mm from the wire surface. The temperature at the wire surface did not increase until ignition because the pyrolysis consumed the input Joule heat. The gas-phase exothermic reaction continued at the front of the pyrolysis gas moving outward to maintain the temperature of the pyrolysis gas until ignition (thermal runaway). In addition, the local oxygen concentration was about 10% at 8.00 s, which provided the mixing condition necessary for ignition than the wire surface, where the local oxygen concentration was less than 5%. Therefore, with a lower current supply, ignition is easier at the pyrolysis gas front than at the wire surface due to the advantage in fuel-oxygen mixing.

In S-2 of Fig. 6 (b) with moderate current supply, the ignition point was also far away from the wire surface, although the ignition occurred after the pyrolysis was completed. For the typical case with a 12 A current, Fig. 7 (b) shows the distributions of HRRPUV, temperature, and reactant fractions along the radial direction around the ignition moment. Ignition occurred at a distance of 15.6 mm from the wire at 1.684 s. This remote ignition at the pyrolysis front implies the same mechanism as in the low current case. In addition, at the moment of ignition (1.684 s), the temperature at the wire surface increased because the core wire was exposed after the pyrolysis was completed at 1.590 s. However, according to the temperature gradient near the wire, such excessive heat from the exposed wire cannot quickly penetrate to support the ignition at the gas front. The lack of oxygen also makes the wire surface region unlikely to ignite. Even if the exposed core wire provides excessive heat in the moderate current cases, the mixture around the front of the pyrolysis gas still has the advantage of ignition far from the wire.

In the high current applied cases (the "wire assisted ignition" regime), ignition occurred after the pyrolysis completion. For the 18 A current case, Fig. 7 (c) shows the distributions of HRRPUV, temperature, and volume fractions of oxygen and ethylene along the radial direction around the ignition moment. As shown by the HRRPUV profiles, the near-surface ignition can be found at 0.806 s after the core wire exposure, but no spontaneous ignition was observed in the gas phase far from the wire. The temperature profiles indicate the excessive heat supply from the wire surface after pyrolysis, but the temperature at the pyrolysis gas front did not rise even with a weak exothermic reaction. The steep temperature gradient indicates the large conductive heat loss at the pyrolysis gas front in comparison with the other two cases in lower currents. The large heat loss prolonged the delay time of spontaneous ignition and can even overcome the local exothermic reaction so that the spontaneous ignition never occurs. Meanwhile, with the inward oxygen diffusion after pyrolysis, the hot wire surface had an advantage to ignite the adjacent gas mixture comparing with the pyrolysis gas front. Subsequently, the flame propagated outward from the wire surface and sequentially ignites the pyrolysis gas away from the wire, as shown in the Fig. 4 (b).

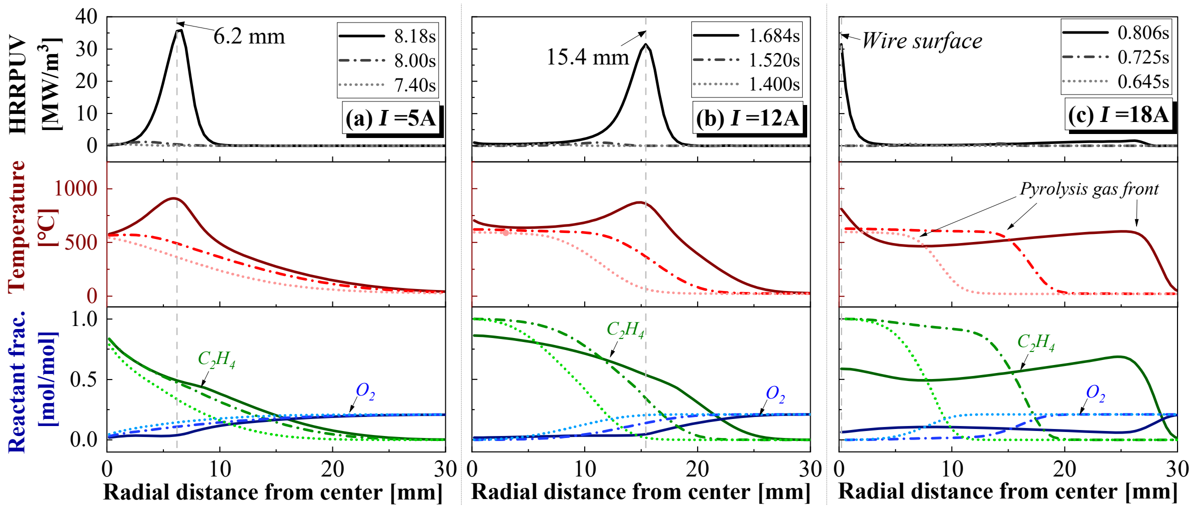

Fig. 7. Radial distributions of HRRPUV, temperature and reactant fractions near the moments of ignition with different applied currents: (a) $I = 5$ A; (b) $I = 12$ A; (c) $I = 18$ A.

The characteristics of the two ignition modes can be identified from the radial distributions as discussed above, which implies that there is a competition between the local reaction time at the wire surface and the pyrolysis gas front. Spontaneous ignition occurs when the pyrolysis gas front reaches the ignition criteria earlier than the gases near the wire surface, otherwise, wire assisted ignition occurs. To clarify the timing difference, we plot the time histories of O_2 fraction, instantaneous velocity, solid temperature (T_s), and gas phase temperature (T_g) on the wire surface for the 5 A, 12 A, and 18 A applied current cases in Fig. 8, the vertical dotted lines in orange color indicate the t_{ig} in all the cases. Using the Device function (DEVC) of FDS [18], O_2 fraction, velocity, and gas temperature data were recorded by gas phase devices at the first cell adjacent to the wire surface boundary; surface temperature was recorded by the solid phase device on the wire surface. As the greater heat loss at the pyrolysis front was confirmed for the 18 A case, the ejection velocity of the pyrolysis gas would be the dominant factor in a quiescent microgravity environment. In Fig. 8 (a), the instantaneous velocities of the pyrolyzed gas from the wire surface under the currents of 5 A, 12 A, and 18 A showed significant differences in the order of magnitude. The 18 A applied current led to a much higher ejected velocity than other cases because the large Joule heat accelerated the pyrolysis reaction leading to a higher mass flux of pyrolysis gas. Due to the faster diffusion of the hot pyrolysis gas into the cold ambient air, the conductive heat loss became comparable with the reaction heat release at the hot gas front, which loses the chance of spontaneous ignition.

Combining the O_2 fraction change near the wire surface in Fig.8 (a) and the corresponding temperature profiles in Fig. 8 (b), the possibilities of ignition on the wire surface in the three scenarios can be confirmed. There are two plateaus in the temperature curves, the melting process at about 120 °C, and the pyrolysis process in the gray shadow (about 500~700°C). After pyrolysis, the exposed core wire made the surface temperature suddenly increase. In the 5 A case, the anaerobic environment ($O_2\% < 2\%$) with a low T_s during pyrolysis unlikely leads to a surface ignition. In the 12 A case, although the surface O_2 started to increase after pyrolysis, it was still limited ($O_2\% < 2\%$), and the lower T_g after ignition implied that there was no flame occurring at the wire surface. In the 18 A case, the hot surface heated the adjacent gases ($T_s > T_g$) after the pyrolysis, and the corresponding $O_2\%$ rose to 6.5% (due to inward diffusion) until the ignition occurred. The largest values of T_s and $O_2\%$ in the 18 A case show the highest ignition probability on the wire surface, and the subsequent T_g jump indicates the successful wire assisted ignition. Here, the exposed wire can act as an additional external heat source assisting the surface ignition at a lower local oxygen level, identified as the wire assisted ignition. Therefore, the transition from the spontaneous ignition to the wire assisted ignition can be explained as the lengthened reaction time on the pyrolysis gas front and shortened reaction time near the wire surface. The former has sufficient mixing but an increasing heat loss, the latter has a sufficient heat input waiting for the oxidizer diffusion.

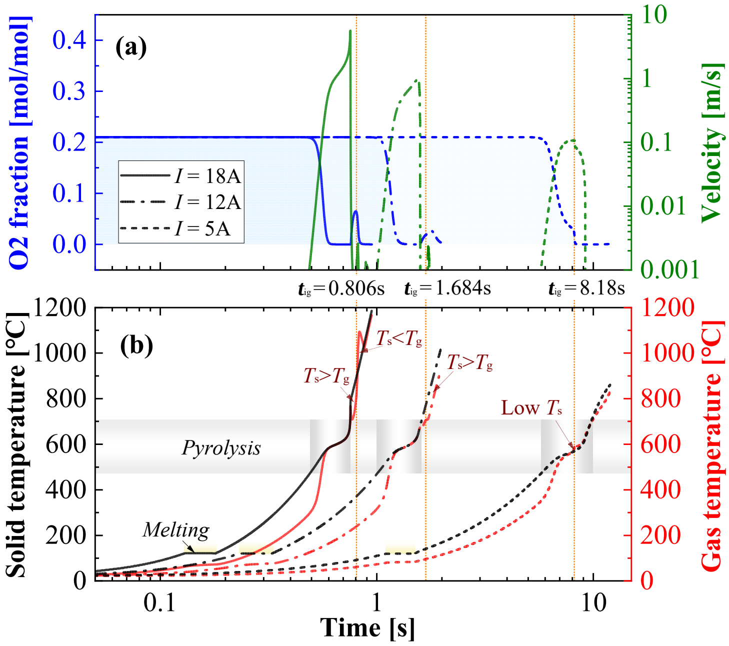

Fig. 8. Time histories of (a) O_2 fraction and instantaneous velocity, (b) solid and gas phase temperatures on the wire surface, for the cases with applied current of 5A, 12A and 18A.

4.4 Ignition energies

Knowing how much energy it takes for an overload ignition helps assess the fire risk in microgravity. Figure 9 (a) shows the ignition energy from the continuous overloading with different electric currents, which is defined as the Joule heat required from the beginning to the t_{ig}. The ignition energy showed a non-monotonical increase with the applied current, where the minimum ignition energy (MIE) was consumed with the 5.5 A current supply. Both simulation and experimental results show that the "spontaneous ignition" regime requires less ignition energy than the "wire-assisted ignition" regime, which implies its higher fire risk. In the "wire assisted ignition" regime, almost all of the energy required for ignition is contributed by Joule heat, while in the "spontaneous ignition" regime, continuous exothermic reactions also contribute to ignition in addition to Joule heat.

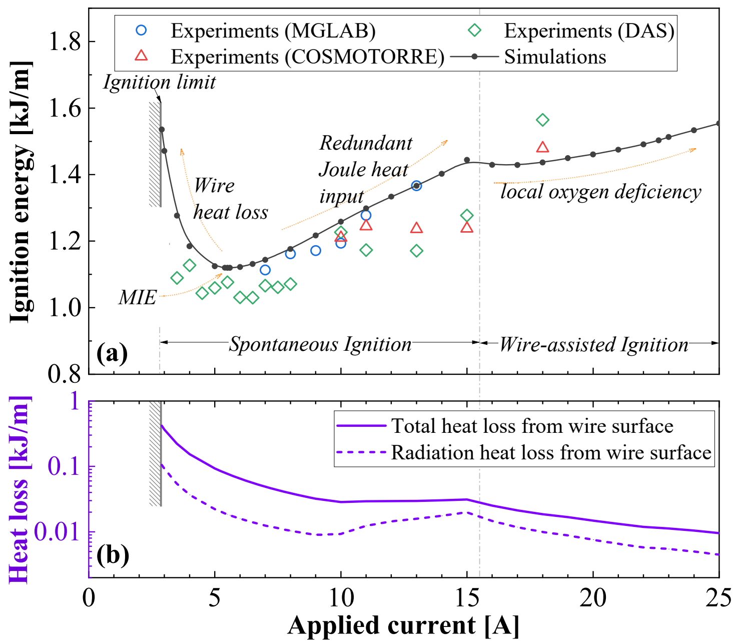

Fig. 9. Energy consumption and heat loss before the ignition as a function of applied current: (a) Ignition energy comparison between μ*G* experiments and 2-D simulations, (b) Total and radiation heat loss from the wire surface.

According to the simulation results lower than 5.5 A, as the applied current decreases approaching the ignition limit, more energy is required for ignition. This tendency agrees with the results of our previous study [17], which is caused by the excessive heat losses from the wire insulation surface when the ignition delay time becomes exponentially longer with a current decrease (as shown in Fig. 5). Similar to the previous numerical work [17], the radiative heat flux from the wire surface became more dominant when the time approaching to the ignition delay time, as shown in the Fig. S.6. in the Supplementary material (S.4). When the pyrolysis starts, the ratio of the radiative heat flux shows a remarkable increase with time. The total radiative heat loss from the wire surface can be counted as the integrated radiative heat flux from beginning of the current supply to the ignition. The radiative and total heat loss from the wire surface was plotted as a function of the applied current until ignition, which is added to Fig. 9 (b). It was found that with a lower applied current, both total and radiative heat loss increase significantly.

By contrast, when the current is higher than 5.5 A, the ignition energy from continuous overloading increases with the applied current increase. As shown in Fig. 5, the decrement of ignition delay time becomes much smaller after the applied current exceeds 5.5 A, and the shorter time differences weaken the importance of heat losses from the wire surface. For the "spontaneous ignition" regime, when the ejected pyrolysis gases react with the ambient air far from the wire surface, Joule heat is continuously supplied from the wire surface. Such additional Joule heat cannot contribute to the spontaneous ignition far away due to the slow thermal diffusion in microgravity. Therefore, with the applied current increasing, more redundant Joule heat is released to increase ignition energy from overloading.

For the “wire assisted ignition” regime, spontaneous ignition cannot happen due to more heat loss from the pyrolysis gas; thus, it requires excessive Joule heat to ignite the adjacent gas with insufficient oxygen. As a result, a slower inward oxygen diffusion may require higher ignition energy to compensate for the local oxygen deficiency. The tendency implied that if we apply the electric current shorter than the ignition delay time, the spontaneous ignition might also happen in microgravity. The short-term ignition in microgravity have been reported by the previous experimental work [15], and it will be investigated numerically in the future.

It should also be noted that due to the limitations and difficulties of microgravity experiments, the core wire gauge was kept constant (0.5 mm diameter) to ensure a sufficiently large Joule heat at a reasonable current intensity. Therefore, using the applied current as the variable for the above analysis may lead to more intuitive results than the applied power. Although we compromised on the choice of wire gauge in the experiment, numerical simulations with different core wire diameters and insulation thicknesses will be performed in the future to investigate the geometry effect.

5. Conclusions

By performing the two-dimensional simulations, the overload ignition of polymer-insulated wire in microgravity with various current values was investigated. The results of the 2-D simulation model showed a good agreement with experimental results in terms of ignition behaviors and ignition delay times. Different ignition positions indicated two ignition modes, one is away from the wire and the other is next to the wire surface.

From the detailed analysis of simulation results, ignition happened away from the wire in low and middle current cases whether or not pyrolysis was completed. In this regime, the hot pyrolysis gas and ambient air mixed much better in the outer region than near the wire surface, the exothermic reaction dominated the ignition at the pyrolysis gas front. This ignition mode was defined as “Spontaneous ignition”. On the other hand, in high current cases, the delay time of spontaneous ignition was prolonged by the large conductive heat loss at the pyrolysis gas front; meanwhile, the exposed core wire with excessive Joule heat had an advantage to ignite the surrounding mixture adjacent to the wire surface earlier. Such ignition mode was defined as “Wire assisted ignition.”

The ignition energy from overloading with the applied current showed a “V” shape curve. The “spontaneous ignition” required less input energy from overloading than the “wire assisted ignition” because not only Joule heat but also reaction heat contributed. With the applied current of 5.5 A, the MIE was found with both small radiative heat loss and redundant Joule heat generation, implying its high risk of a fire accident in space.

Acknowledgements

This research was supported by JAXA as a candidate experiment for the third stage use of JEM/ISS titled “Evaluation of gravity impact on combustion phenomenon of solid material toward higher fire safety” (called “FLARE”). This work used computational resources of the supercomputer Fugaku provided by RIKEN through the HPCI System Research Project (Projects ID: hp220286, hp220395). The authors express sincere words of gratitude to Yasuhiro Kido (Hokkaido University) and Kohei Shimizu (Hokkaido University) for their contributions in the μ*G* experiments.

References

[1] S. McAllister, C. Fernandez-Pello, D. Urban, G. Ruff, Piloted ignition delay of PMMA in space exploration atmospheres, Proc. Combust. Inst. 32 II (2009) 2453–2459. https://doi.org/10.1016/j.proci.2008.05.076.

[2] S. McAllister, C. Fernandez-Pello, D. Urban, G. Ruff, The combined effect of pressure and oxygen concentration on piloted ignition of a solid combustible, Combust. Flame. 157 (2010) 1753–1759. https://doi.org/10.1016/j.combustflame.2010.02.022.

[3] O. Fujita, J. Takahashi, K. Ito, Experimental study on radiative ignition of a paper sheet in microgravity, Proc. Combust. Inst. 28 (2000) 2761–2767. https://doi.org/10.1016/s0082-0784(00)80697-9.

[4] J. Takahashi, O. Fujita, K. Ito, The effect of irradiation angle on laser ignition of cellulose sheet in microgravity, Proc. Combust. Inst. 30 II (2005) 2311–2317. https://doi.org/10.1016/j.proci.2004.08.097.

[5] Y. Nakamura, H. Yamashita, T. Takeno, G. Kushida, Effects of gravity and ambient oxygen on a gas-phase ignition over a heated solid fuel, Combust. Flame. 120 (2000) 34–48. https://doi.org/10.1016/S0010-2180(99)00077-2.

[6] S.. L. Olson, T. Kashiwagi, O. Fujita, M. Kikuchi, K. Ito, Experimental observations of spot radiative ignition and subsequent three-dimensional flame spread over thin cellulose fuels, Combust. Flame. 125 (2001) 852–864. https://doi.org/10.1016/S0010-2180(00)00249-2.

[7] Y. Nakamura, T. Kashiwagi, S.L. Olson, K. Nishizawa, O. Fujita, K. Ito, Two-sided ignition of a thin PMMA sheet in microgravity, Proc. Combust. Inst. 30 II (2005) 2319–2325. https://doi.org/10.1016/j.proci.2004.07.037.

[8] R. Friedman, Fire safety in spacecraft, Fire Mater. 20 (1996) 235–243. https://doi.org/10.1002/(SICI)1099-1018(199609)20:5<235::AID-FAM580>3.0.CO;2-Y.

[9] NASA_NHB8060.1C, Flammability, odor, offgassing, and compatibility requirements and test procedures for materials in enbironments that support combustion, (1991).

[10] Y. Kobayashi, Y. Konno, X. Huang, S. Nakaya, M. Tsue, N. Hashimoto, O. Fujita, C. Fernandez-Pello, Laser piloted ignition of electrical wire in microgravity, Proc. Combust. Inst. 37 (2019) 4211–4219. https://doi.org/10.1016/j.proci.2018.06.089.

[11] M. Nagachi, F. Mitsui, J.-M. Citerne, H. Dutilleul, A. Guibaud, G. Jomaas, G. Legros, N. Hashimoto, O. Fujita, Effect of Ignition Condition on the Extinction Limit for Opposed Flame Spread Over Electrical Wires in Microgravity, Fire Technol. 56 (2020) 149–168. https://doi.org/10.1007/s10694-019-00860-6.

[12] S. Xue, W. Kong, Smoke emission and temperature characteristics of the long-term overloaded wire in space, J. Fire Sci. 37 (2019) 99–116. https://doi.org/10.1177/0734904118821665.

[13] W. Kong, K. Wang, W. Xia, S. Xue, Ignition and Combustion Characteristics of Overloaded Wire Insulations Under Weakly Buoyancy or Microgravity Environments, in: Res. Dev., 2019: pp. 191–235. https://doi.org/10.1007/978-981-13-1340-0_9.

[14] K. Agata, O. Fujita, Y. Ichimura, T. Fujii, H. Ito, Y. Nakamura, Wire Insulation Ignition with Excess Electric Current in Microgravity, J. Japan Soc. Microgravity Appl. 25 (2008) 11–16.

[15] O. Fujita, T. Kyono, Y. Kido, H. Ito, Y. Nakamura, Ignition of electrical wire insulation with short-term excess electric current in microgravity, Proc. Combust. Inst. 33 (2011) 2617–2623. https://doi.org/10.1016/j.proci.2010.06.123.

[16] Y. Takano, O. Fujita, N. Shigeta, Y. Nakamura, H. Ito, Ignition limits of short-term overloaded electric wires in microgravity, Proc. Combust. Inst. 34 (2013) 2665–2673. https://doi.org/10.1016/j.proci.2012.06.064.

[17] K. Shimizu, M. Kikuchi, N. Hashimoto, O. Fujita, A numerical and experimental study of the ignition of insulated electric wire with long-term excess current supply under microgravity, Proc. Combust. Inst. 36 (2017) 3063–3071. https://doi.org/10.1016/j.proci.2016.06.134.

[18] K. McGrattan, S. Hostikka, R. McDermott, J. Floyd, M. Vanella, Fire Dynamics Simulator User's Guide, Gaithersburg, MD, 2018. https://doi.org/10.6028/NIST.SP.1019.

[19] F. Guo, S. Kawaguchi, N. Hashimoto, O. Fujita, Effect of pyrolysis kinetic parameters on the overload ignition of polymer insulated wires in microgravity, Proc. Combust. Inst. 39 (2023) 3939–3947. https://doi.org/10.1016/j.proci.2022.08.087.

[20] K.B. McGrattan, S. Hostikka, J. Floyd, M. Vanella, Fire Dynamics Simulator Technical Reference Guide Volume 1: Mathematical Model, Gaithersburg, MD, 2018. https://doi.org/10.6028/NIST.SP.1018.

[21] J. Brandrup, E.H. Immergut, E.A. Grulke, Polymer Handbook, 4th ed., Wiley, 2003.

[22] R.D. MFG., Melt Density Data, (2021). https://www.rdray.com/melt-density (accessed June 30, 2021).

[23] W.N. dos Santos, Thermal properties of melt polymers by the hot wire technique, Polym. Test. 24 (2005) 932–941. https://doi.org/10.1016/j.polymertesting.2005.06.001.

[24] M.Y. Keating, C.S. Mclaren, Thermal conductivity of polymer melts, Thermochim. Acta. 166 (1990) 69–76. https://doi.org/10.1016/0040-6031(90)80170-4.

[25] T. Okada, R. Ishige, S. Ando, Analysis of Thermal Radiation Properties of Polyimide and Polymeric Materials Based on ATR-IR spectroscopy, J. Photopolym. Sci. Technol. 29 (2016) 251–254. https://doi.org/10.2494/photopolymer.29.251.

[26] Optotherm Support, Emissivity in the Infrared, (2022). https://www.optotherm.com/emissivity.

[27] A. Tewarson, R.F. Pion, Flammability of plastics—I. Burning intensity, Combust. Flame. 26 (1976) 85–103. https://doi.org/10.1016/0010-2180(76)90059-6.

[28] C.K. Westbrook, F.L. Dryer, Simplified Reaction Mechanisms for the Oxidation of Hydrocarbon Fuels in Flames, Combust. Sci. Technol. 27 (1981) 31–43. https://doi.org/10.1080/00102208108946970.

[29] I. Glassman, R. Yetter, Spontaneous ignition temperature data, in: Combustion, Elsevier, 2015: pp. 705–729. https://doi.org/10.1016/B978-0-12-407913-7.15008-X.

[30] Y. Nakamura, T. Kashiwagi, Effects of sample orientation on nonpiloted ignition of thin poly(methyl methacrylate) sheet by a laser, Combust. Flame. 141 (2005) 149–169. https://doi.org/10.1016/j.combustflame.2004.12.014.

[31] T. KASHIWAGI, A Radiative Ignition Model of a Solid Fuel, Combust. Sci. Technol. 8 (1973) 225–236. https://doi.org/10.1080/00102207308946646.

[32] Y. NAKAMURA, T. TAKENO, Appropriate Criterion of Spontaneous Ignition of an Externally Heated Solid Fuel in Numerical Study, JSME Int. J. Ser. B. 44 (2001) 288–298. https://doi.org/10.1299/jsmeb.44.288.

Figure captions

Fig.1. Experimental setup (a) schematic of experimental chamber, (b) overview picture.

Fig. 2. Schematics of the 2-D computational domain.

Fig. 3. Experimental images of wire ignition with applied current of (a) 5 A recorded by backlight image; (b) 18 A recorded by direct image.

Fig. 4. Simulation images of wire ignition represented by HRRPUV with applied current of (a) 5 A and (b) 18 A.

Fig. 5. Comparison of ignition delay times between μ*G* experiments and 2-D simulations as a function of applied current.

Fig. 6. Transition of two ignition modes as a function of applied current: (a) ignition position; (b) ratio of ignition delay time and pyrolysis completion time.

Fig. 7. Radial distributions of HRRPUV, temperature and reactant fractions near the moments of ignition with different applied currents: (a) $I = 5$ A; (b) $I = 12$ A; (c) $I = 18$ A.

Fig. 8. Time histories of (a) O_2 fraction and instantaneous velocity, (b) solid and gas phase temperatures at the wire surface, for the cases with applied current of 5A, 12A and 18A.

Fig. 9. Energy consumption and heat loss before the ignition as a function of applied current: (a) Ignition energy comparison between μ*G* experiments and 2-D simulations, (b) Total and radiation heat loss from the wire surface.